UC Merced
UC Merced Previously Published Works

Title

Automated Measurement of Spatially Resolved Hair–Hair Single Fiber Adhesion

Permalink

Journal

ISSN

Authors

Cristiani, Thomas R
Cadirov, Nicholas A
Zhang, Zhanping
et al.

Publication Date

2019-12-03

DOI

Peer reviewed

Automated Measurement of Spatially Resolved Hair−Hair Single Fiber Adhesion

Thomas R. Cristiani,*[†,‡,∥] Nicholas A. Cadirov,[§,∥] Zhanping Zhang,[⊥] Zhiwei Shi,[⊥] Andrei Bureiko,[⊥] Roberto C. Andresen Eguiluz,[§,∥,#] Kai Kristiansen,[§,○] Jeffrey Scott,[○] Knut Meinert,[●] Peter H. Koenig,[⊥] and Jacob N. Israelachvili[†,‡,§,○,△]

[†]Materials Department, [‡]Materials Research Laboratory, and [§]Department of Chemical Engineering, University of California, Santa Barbara, California 93106, United States
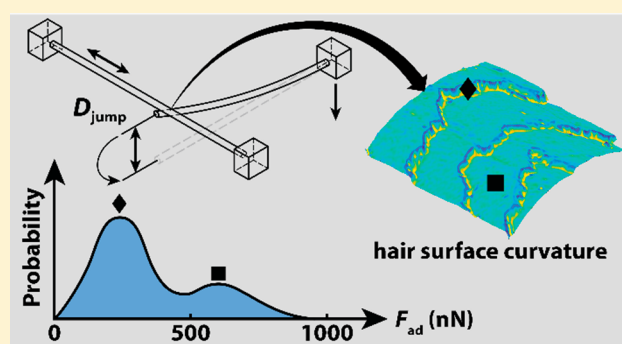
[⊥]The Procter and Gamble Company, Mason Business Center, 8700 Mason-Montgomery Road, Mason, Ohio 45040, United States

[○]SurForce LLC, 354 South Fairview Avenue, Suite B, Goleta, California 93117-3629, United States

[●]Procter & Gamble Service GmbH, Sulzbacher Str. 40, 65824 Schwalbach am Taunus, Germany

Ⓢ *Supporting Information*

ABSTRACT: The adhesion force between individual human hair fibers in a crosshair geometry was measured by observing their natural bending and adhesive jumps out of contact, using optical video microscopy. The hair fibers' natural elastic responses, calibrated by measuring their natural resonant frequencies, were used to measure the forces. Using a custom-designed, automated apparatus to measure thousands of individual hair−hair contacts along millimeter length scales of hair, it was found that a broad, yet characteristic, spatially variant distribution in adhesion force is measured on the 1 to 1000 nN scale for both clean and conditioner-treated hair fibers. Comparison between the measured adhesion forces and adhesion forces modeled from the hairs' surface topography (measured using confocal laser profilometry) shows they have a good order-of-magnitude agreement and have similar breadth and shape. The agreement between the measurements and the model suggests, perhaps unsurprisingly, that hair−hair adhesion is governed, to a first approximation, by the unique surface structure of the hairs' cuticles and, therefore, the large distribution in local mean curvature at the various individual contact points along the hairs' lengths. We posit that haircare products could best control the surface properties (or at least the adhesive properties) between hairs by directly modifying the hair surface microstructure.

■ INTRODUCTION

Healthy, shiny, smooth, and soft hair is desired by many people in different cultures around the world. However, due to aging from mechanical and chemical damage, the morphology and chemistry of the hair fibers' layered outer cuticles become nonuniform and deviate from their natural virgin properties.[1,2] To mask, prevent, or otherwise reverse the effects of this aging, hair products, such as conditioners and other chemical treatments, have been designed to modify hair surfaces with lipids or adsorbed polymers, such as silicones and waxes.[3] These surface-modifying layers can range in thickness from 1s to 100s of nanometers and function by changing the surface energy and normalizing the micro/nanostructure of hairs' outer layers.[4,5] Due to the biodiversity of human hair across various ethnicities and age groups, formulating haircare products that can accomplish these tasks with similar efficacy, independent of the individual using the product, is a significant technological challenge.[3] It is also difficult to predict how surface treatments will influence the overall "manageability" of an individual's unique head of hair.

Within the last 15 to 20 years, evaluating the efficacy of haircare products has involved correlating consumer surveys regarding the look and feel of untreated and treated hairs (both virgin and damaged) with the treatments' formulas and their effects on the hairs' surface properties, such as friction and adhesion.[1,2,4−8] Reducing interfiber friction and adhesion benefits long-term hair health by reducing wear, breakage, and combing forces. However, other more subjective aspects of haircare, such as styling and style retention, are more subtly dependent on hair surface properties and do not necessarily benefit directly from minimizing friction and adhesion.
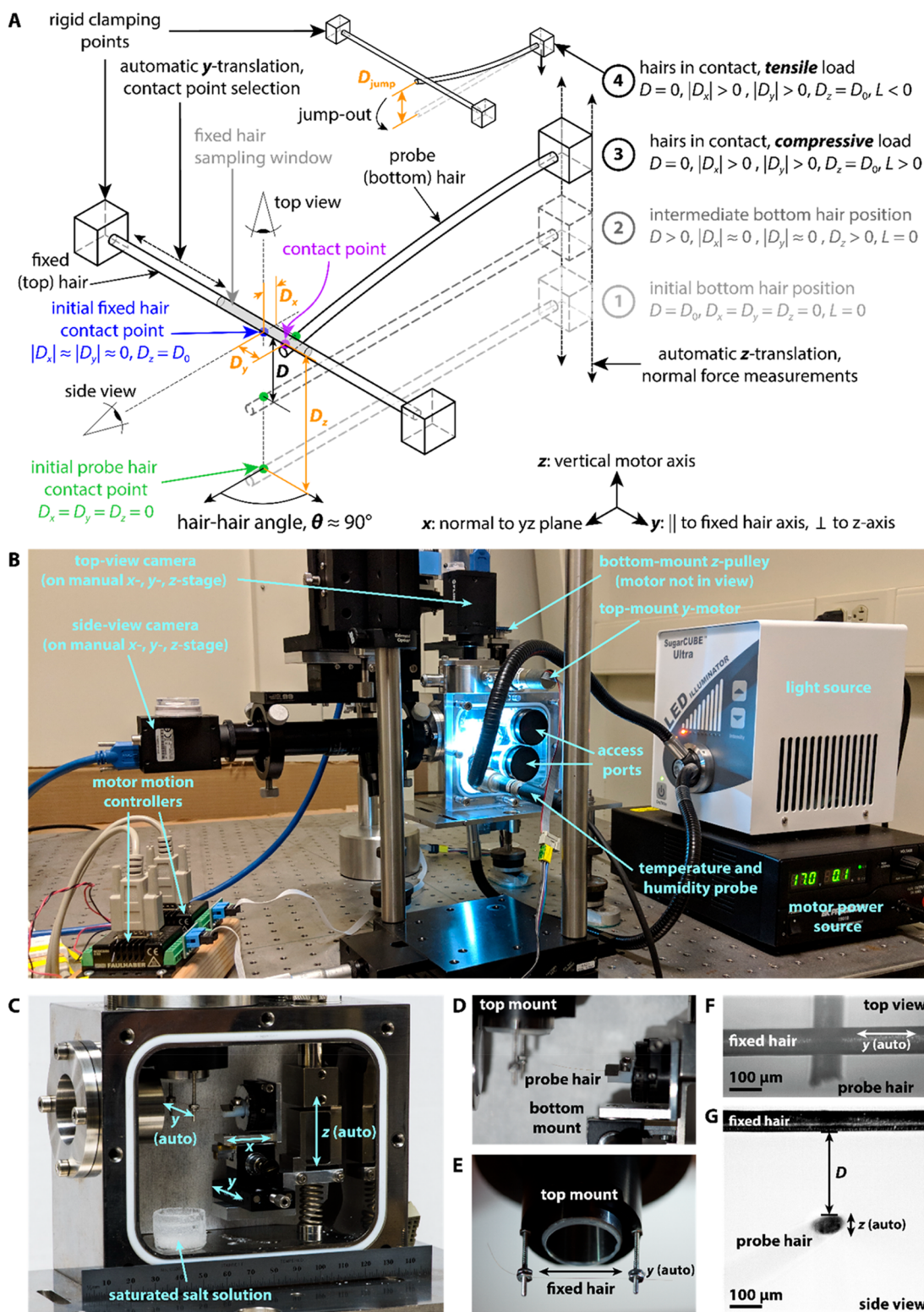
Figure 1. Schematic and photos of experimental apparatus. (A) A schematic representation of the two interacting hair fibers on their respective mounts and translational stages. The probe hair is depicted in four states: (1) its initial position out of contact, (2) an intermediate position during approach toward contact, (3) under compressive load, L, while in contact (the contact position on both the probe and the fixed hair may have changed from the green and blue circles to the purple circle during compression), and (4) under tensile load, L, while in contact before an adhesive jump out (indicated by D_{jump}). Also, shown are the definitions for the coordinate system, the views from the top- and side-view cameras, and the definitions of the relative x-, y-, and z-positions, D_x, D_y, and D_z, of the probe hair with respect to its initial position and the hair—hair separation distance, D. (B) Labeled photograph of the overall HAFA setup. (C) Photograph of the inside of the HAFA chamber depicting the various motion control components for the probe hair. (D, E) Photographs of the bottom and top mounts with hairs affixed. (F, G) Micrographs from the top- and side-view cameras depicting the probe and fixed hairs out of contact at some separation distance, D.

Much of the previous work on characterizing the surface properties of hair, especially hair adhesion, has been conducted using asymmetrical systems, whereby atomic force microscope (AFM) cantilevers with high (10s of nm radii) and low (10s of μm radii) curvature tips are rasterized around small areas of the hairs' surfaces.[1,2,5,6,9−14] From these experiments, the spatial variations in surface energies of treated and untreated, virgin and damaged hair can be calculated.

To use the information gained from conducting microscopic physical measurements in a more cost-effective and rapid way, it would be useful to somehow translate the physical information to accurate computer models, in which full heads of hair can be simulated and altered according to damage and treatment. However, due to the complexity of the cuticle geometry, it is difficult to extrapolate these microscopic measurements to model the behavior of full heads of hair[15] with millions of individual fiber−fiber interactions.

Therefore, to translate microscopic surface properties to the macroscopic behavior of the physiologically relevant system, it is necessary to measure the forces between pairs of fibers and the variance in forces across various contact locations and hair specimens instead of just measuring the forces between fibers and idealized probes.

Symmetrical hair−hair adhesion and friction experiments have previously been conducted by other research groups by affixing short segments of hair to the ends of tip-less AFM cantilevers.[16−19] Though this method can achieve ~10 pN normal and lateral force resolution, it requires painstakingly precise manipulation of small hair segments whose ends must be cut using either lasers[16] or focused ion beams[17−19] to avoid edge interactions within the AFM.

In this work, to overcome the limitations caused by this complicated sample preparation and the previously discussed minimal range-of-motion available in AFMs, we present an apparatus specifically designed for measuring the adhesion force between fibers, which uses one of the interacting fibers as the force probe (Figure 1A). Similar assays have been used to measure the friction and adhesion of natural fibers[20] and polymer fibers,[21−23] but the natural fiber experiments have been limited to the use of carbon or polymer probes. In the present work, the probe hair fibers are calibrated using various methods, including (i) simply hanging weights of known mass from the end of the probe fiber, (ii) deflecting the fiber against another well-calibrated spring of known constant, and (iii) measuring both the free mass and the natural resonant frequency of the probe fiber, which all agree within <10% variation. Sufficiently long (2−3 cm) probe fibers can achieve effective spring constants, k, at their free ends in the ~1 mN/m (1 nN/μm) range, which is 10^6 and 10^2 times weaker than a typical surface force apparatus (SFA) and AFM cantilevers, respectively.[24−26] Assuming the hairs obey Hooke's law at small displacements, the load exerted by the probe hair is given by $L = k\Delta z$, where Δz is the displacement of the tip of the probe hair from equilibrium. Under this assumption, these weak spring constants allow for the measurement of adhesion forces as low as 1 nN by using a simple, low-resolution video microscope to measure the adhesive jumps, out of contact with ~1 μm resolution.

Adapting the above method for use in a traditional SFA Mark II (SurForce LLC) and taking advantage of the SFA's pre-existing ability to electronically actuate the motion and relative positions of both fibers with submicron accuracy, we can reproducibly measure the adhesion force at highly localized contact points on each hair and automatically sample thousands of individual contact locations to generate overall and spatially resolved adhesion force distributions. The magnitudes and, to some extent, the shapes of these distributions are reproducible and are predicted in this work from a Hertzian asperity model leveraging a combination of surface-topography measurements using laser profilometry and surface energy measurements via fiber tensiometry.[27] The agreement between the measured and the modeled adhesion forces suggests that surface topography is the main cause of the large distributions in adhesion force. We therefore suggest that future hair care products may take advantage of this phenomenon by strategically manipulating the surface morphology of hair fibers.

■ EXPERIMENTAL SECTION

Experimental Apparatus. The experimental apparatus used for this work, dubbed the Hair Adhesion Force Apparatus (HAFA, Figure 1), uses the main chamber, coarse z-control, and friction device top mount from a standard SFA Mark II (SurForce LLC). The SFA has been modified to accommodate a manual motion assembly, including y- and x-translation stages, to which the probe hair is mounted. Figure 1 shows both a schematic and photos of the HAFA and the mounted hairs, defining the coordinate system and specifying the directions which the probe and fixed hairs are automatically actuated. Also shown are the optical axes and views from the top- and side-view cameras.

The main premise of the HAFA technique, and the basis for the modifications to the SFA Mark II, is that a single, fairly straight human hair fiber, when fixed at one end, functions as an elastic cantilever beam with elliptical cross-section (discussed further in "Hair Spring Constant Calibration Methods"). The free end of this "probe hair" is allowed to interact with the surface of another fixed hair fiber in a crosshair configuration (angle between hair axes, $\theta \approx 90°$) and is viewed from the positive z- and x-directions, as defined in Figure 1A. After carefully calibrating the probe hair's spring constant ("Hair Spring Constant Calibration Methods"), the adhesion force between the fibers is calculated by measuring the jump-out distance between the hairs, D_{jump}, after they separate following adhesive contact ("Hair Detection and Distance Measurements").

Discussed further below, the HAFA also allows for control of various interaction time scales and velocities using computer controlled motors which move both the probe hair in the z-direction and the fixed hair in the y-direction. The HAFA, as with all SFAs, is enclosed in an environmentally controlled chamber, where the humidity is controlled using a saturated salt solution within the chamber and the chamber itself is at thermal equilibrium within a water-cooled experimental room. For the experiments presented, the temperature and relative humidity were set at 25 ± 0.5 °C and 65 ± 3%, respectively, and monitored with a computer-connected Rotronic HCA2-S temperature and humidity probe.

Hair Detection and Distance Measurements. Before assigning real-space distances to any objects in either microscope video feed, the microscopes must be calibrated at their focal planes. This was done for each microscope by focusing on a graticule with lines spaced at 100 μm and counting the average number of video pixels between the centers of the grating lines. For all experiments, the focal planes of the side- and top-view cameras are centered at the middle-most cross-section of the fixed hair perpendicular to the viewing direction. The calibrated and focused video feeds are then autocontrast-adjusted so that the top and bottom 1% of all pixel values are saturated. Then, manually selected values for an isotropic Gaussian filter radius, oversaturation filter (essentially a multiplication factor), and Sobel edge detection threshold are applied, forming a binary image of "kept" pixels which denote pixels near the edge of all objects (hairs) in the image. Distances between specified pixels in these binary images are then calculated (Figure 2).

In the side-view video stream, the bottom edge of the probe hair and the top edge of the fixed hair are found by averaging the positions of the pixels within specified z-distances of the extreme top and bottom edges of the "kept" pixels. The difference between these two locations is tracked with time and is represented in Figure 2A. The distance

A - Side-view camera
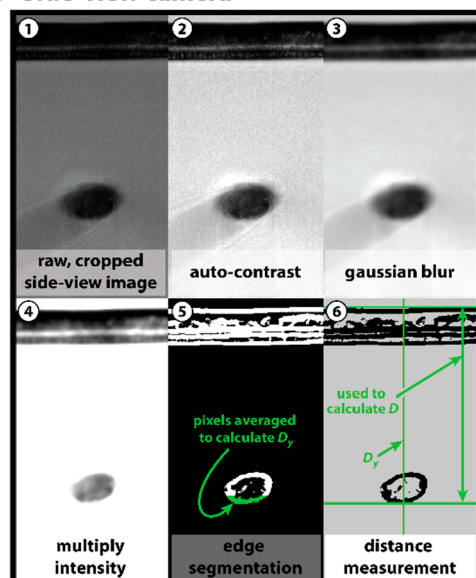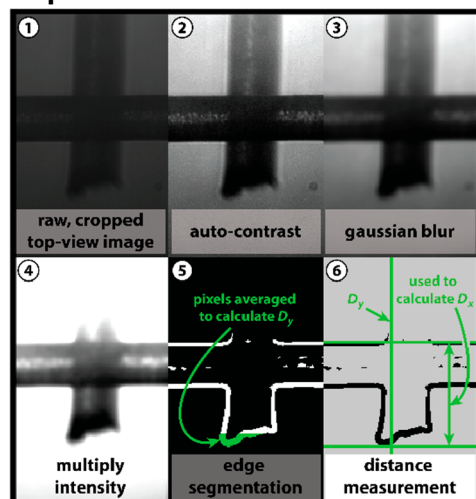

B - Top-view camera

Figure 2. Image processing and distance measurements. Image processing steps (1−6) and distances calculations performed on A) side-view and B) top-view video frames.

between the hairs, D, is therefore taken as this difference minus the minimum value of this difference. The y-position of the probe is taken as the average y-position of the pixels near the extreme bottom edge of the probe (Figure 2A).

In the top-view video stream, a similar image processing algorithm is applied. The x-position of the probe is taken as the average x-position of the pixels near the free tip of the probe relative to the average x-position of the pixels at the far side (negative x) of the fixed hair. The y-position of the probe is taken as the average y-position of the same pixels used to calculate the x-position in the top-view camera. Tracking the position of the probe hair in this manner allows for real-time tracking of the probe hair in all three spatial dimensions, thus, fully defining its motion.

Hair Spring Constant Calibration Methods. Treating the bottom free hair fiber as a simple cantilever beam with an elliptical cross-section whose minor axis is parallel to the z-direction, the deflection of the tip of the beam in the z-direction, Δz, is related to the force, L, applied to or by the cantilever to achieve that deflection by the following relationship:

$$L = k\Delta z$$

where k is the effective spring constant of the hair normal to the direction of deflection at the point where the force is being applied. If the force is applied very near the tip of the hair, then k is related to the dimensions and elastic properties of the cantilever by the following relationship:

$$k = E\left(\frac{3\pi}{4}\right)\left(\frac{a^3 b}{l^3}\right)$$

where E is the elastic modulus of the hair, a and b are the minor and major radii of the elliptical cross-section, respectively, and l is the free length of the hair fiber.

Previous experiments[17] have measured the adhesion force between hair fibers to be on the order of 100 nN. Therefore, to measure subtle variations in adhesion force, a force resolution of ∼1 nN is necessary. A simple 10× microscope objective with a numerical aperture (NA) of 0.25 has an optical resolution of ∼1 μm when paired with a camera having sufficiently small pixels. Therefore, the spring constant, k, of the free hair must be ∼1−10 nN/μm, or ∼1−10 mN/m, to measure these subtle forces using the adhesive jump-out distances from contact, D_{jump}. For a typical Caucasian hair fiber, $a \approx 20−40$ μm, $b \approx 30−50$ μm, and $E \approx 1−10$ GPa. Therefore, to achieve a spring constant of ∼1 nN/μm, the hair length must be between 1 and 3 cm. As such, the experimental apparatus has been designed so that the manual x-translation stage to which the probe hair is mounted can accommodate hairs between 1 and 4 cm in length.

Using these guidelines to design the system ensures the probe hairs are close to the appropriate spring constant; however, each fiber must be physically calibrated before the adhesion force can be measured. The three methods for determining the spring constant employed in this work, which are internally consistent within roughly 10% variance, are

Table 1. Probe Hair Spring Constants Obtained via Resonant Frequency and Reference Spring Methods (Where Applicable)[a]

	resonant frequency method					reference spring method ($k_{ref} = 51.5 \pm 3.7$ nN/μm)		
hair specimen	$l \pm 0.2$ (mm)	$\rho_l \pm 0.05$ (μg/mm)	$m \pm 0.1$ (μg)	f_0 (Hz)	K (nN/μm)	v_a (μm/s)	$v_{a,c}$ (μm/s)	K (nN/μm)
clean hair 1	22.0	7.38	162.4	71.5 ± 3.1	7.3 ± 0.7			
clean hair 2	17.5	6.64	116.2	56.4 ± 1.0	3.51 ± 0.13	30.8 ± 0.3	2.03 ± 0.02	3.6 ± 0.3
clean hair 3	21.0	9.63	202.2	48.1 ± 0.1	4.44 ± 0.02			
clean hair 4	18.0	5.66	101.9	52.6 ± 0.2	2.67 ± 0.02			
clean hair 5	21.0	7.13	149.8	49.6 ± 0.2	3.50 ± 0.02	29.7 ± 0.2	1.98 ± 0.03	3.7 ± 0.3
clean hair 6	24.0	5.18	124.2	33.4 ± 1.0	1.31 ± 0.02			
clean hair 7	19.5	10.16	198.2	75.5 ± 0.6	10.7 ± 0.2			
clean hair 8	20.5	4.72	96.7	37.0 ± 1.0	1.25 ± 0.02			
treated hair 1	21.2	7.24	153.4	41.3 ± 0.5	2.48 ± 0.02	32 ± 0.1	1.54 ± 0.02	2.6 ± 0.2
treated hair 2	23.5	7.42	174.3	36.2 ± 0.1	2.16 ± 0.06	31.7 ± 0.1	1.34 ± 0.03	2.3 ± 0.2

[a]Intervals on each k and f_0, v_a, and $v_{a,c}$ are 95% confidence bounds; intervals on l, ρ_l, and m are instrument resolution.

detailed below (Table 1 and Figures 3−5). Because of the similarities between each method, for most of the experiments presented in this work, the "fundamental resonant frequency" method below was used.

Suspended Masses. The most conceptually straightforward way of calibrating the spring constant of the probe hair is by hanging from its end small weights of known mass. Small coils of 96 μm diameter Nylon fishing line of various total lengths were used for this purpose and were massed using a Mettler Toledo UMX2 microbalance ($\pm$0.1 μg). The

Figure 3. "Suspended mass" method spring constant calibration curves for (A) a hair cantilever used during validation, (B) a PVC reference spring, and (C) a nylon reference spring. Error ranges are 95% confidence intervals for the dashed best-fit lines. (D) Schematic representation of the hanging mass method showing the cantilever before (gray, dashed) and after (black, solid) a hanging weight, w, is positioned at its free end. D_z is the displacement of the tip of the cantilever between the "force-free" position and the position with the hanging mass.

slope of the best fit line, passing through the origin, of the deflection of the probe hair, Δz, versus the weight of the masses, w, is taken as the spring constant. This method is, however, the most difficult to implement in practice. Figure 3 shows the calibration of a hair used to validate this method as well as the calibrations of Nylon and PVC reference springs used for the calibration method described in the next section.

Reference Spring. Alternatively, the hair may be calibrated against a reference cantilever of known spring constant (which can be calibrated by either of the methods described above or below). This method involves moving the probe hair at a constant z-velocity while tracking both the z-position of the probe hair and the z-position of the reference spring (Figure 4). By computing the deflection of the probe hair and reference spring using their velocities and time in contact, it is straightforward to show that the spring constant of the probe hair is given by

$$k = k_{ref}\frac{v_{a,c}}{v_a - v_{a,c}}$$

where k_{ref} is the spring constant of the reference spring, v_a is the free velocity during approach to contact of the probe hair before it interacts with the reference spring, and $v_{a,c}$ is the velocity of the probe hair (and subsequently the reference spring) while in contact. Two reference springs were used in these experiments: (i) a segment of the same nylon fishing line used to fashion the hanging masses in the previous section, and (ii) a shim of poly(vinyl chloride) (PVC) measuring approximately 50 μm thick, 500 μm wide, and 18 mm long. The reference springs were calibrated using the "suspended masses" method and their calibration curves and spring constants are given in Figure 3.

This method, though reproducible, is greatly affected by the relative orientations of the probe hair and the reference spring and could potentially damage the contact region of the probe hair due to sliding between the hair and reference spring during loading and unloading. It is also limited by the accuracy with which the reference spring has been calibrated.

Fundamental Resonant Frequency. Finally, the method used for most of the presented adhesion force measurements involves using a camera capable of sampling at 300 frames per second to measure the fundamental resonant frequency of the probe hair as it freely vibrates after an adhesive jump out. Treating the probe hair as an isotropic cantilever beam with a uniform elliptical cross-section (a rough approximation, discussed above), this fundamental frequency is related to the spring constant of the probe hair by[28]

$$f_0 = \frac{C}{2\pi}\sqrt{\frac{k}{0.24m}}$$

where f_0 is the fundamental resonant frequency of the probe hair, C is a shape constant that depends on the mode of vibration, and m is the mass of the entire free length of the probe hair. For these experiments, given that the probe hair is resonating freely and is not being driven by a resonating actuator, the mode of vibration is the first harmonic (or mode 1, with zero nodes) and, therefore, $C = 1$.

The mass of the free length of the fiber is determined by first weighing the unmounted fiber on a Mettler Toledo UMX2 microbalance ($\pm$0.1 μg) and measuring its length with a standard metric ruler ($\pm$0.25 mm). The ratio of mass/length, ρ_l, is assumed constant for the fiber. After mounting the fiber and cutting it to the appropriate length for the measurement ($\sim$15 to 30 mm), the free length, l_{free}, is measured and the free mass is assumed to be $m = \rho_l l_{free}$.

To determine the resonant frequency of the probe hair, several videos of individual adhesive jumps out are recorded and the interhair distances are measured for each according to the procedure detailed in "Hair Detection and Distance Measurements". The continuous wavelet transform of $D(t)$, giving its temporally localized frequency response, is then computed using MATLAB's built-in Wavelet Toolbox. The fundamental frequency of the probe fiber is computed as the frequency component of the wavelet transform with the highest power, or amplitude, in the temporal vicinity of the adhesive jump out (Figure 5) associated with the "ring-down" frequency of the underdamped spring
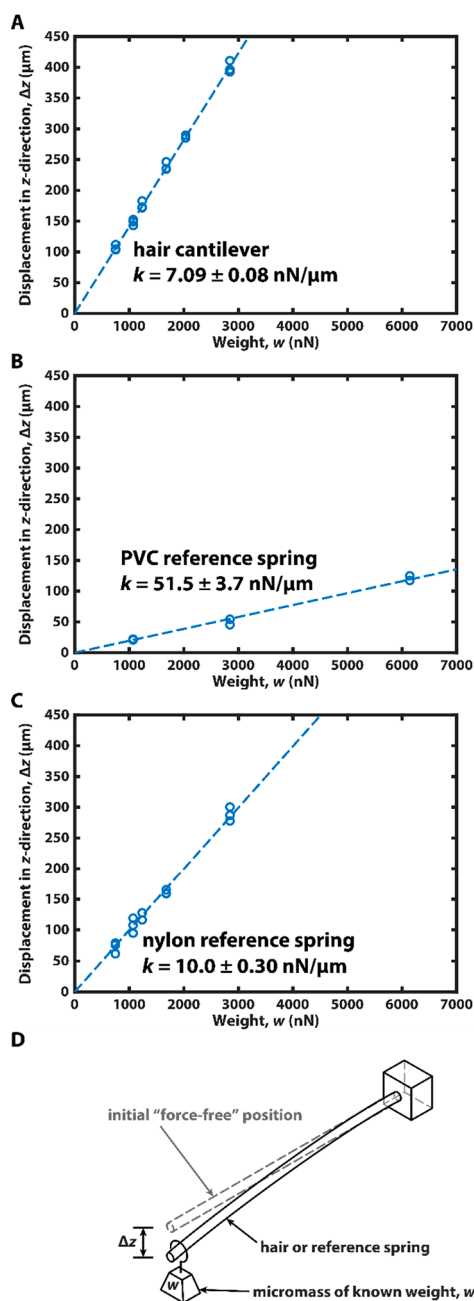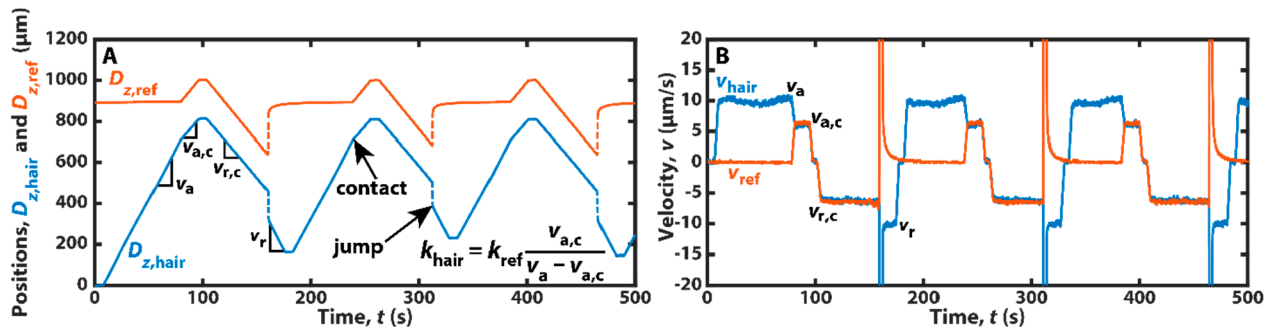
Figure 4. Reference spring calibration method. The position (A) and velocity (B) traces for both a hair cantilever (blue) and nylon reference spring (orange) used to validate the reference spring constant calibration method. Three separate loading and unloading cycles are shown, from which the hair's spring constant is calibrated. For this experiment, $k_{ref} = 10.0 \pm 0.3$ nN/μm (Figure 3C), $v_a \approx 10.0\,\mu$m/s, and $v_{a,c} \approx 6.0\,\mu$m/s; therefore, $k_{hair} \approx 15.0 \pm 0.5$ nN/μm.
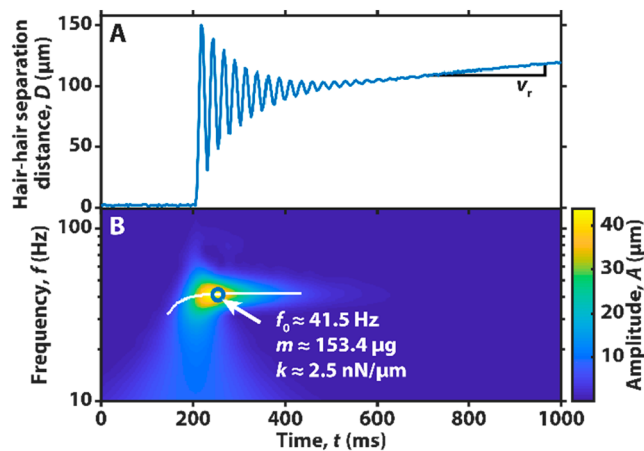

Figure 5. Resonant frequency calibration method. (A) Hair−hair separation distance, D, as a function of time, t, for an adhesive jump-out of the probe hair segment of "Treated Hair 1". The characteristic "ring-down" of the under-damped system is clearly visible between 200 and 600 ms. (B) Frequency spectra of $D(t)$ computed using a continuous wavelet transform. The fundamental frequency, f_0, is indicated by the open circle and is determined by averaging points along the white peak amplitude trace near where it levels off. The free mass of the probe hair segment, m, and the calculated spring constant, k, for this measurement are also indicated.

system. We find this frequency determination to be highly reproducible (±0.2 to 4% over 5 to 6 videos). Table 1 lists the spring constants for the hairs presented in this study and demonstrates, where applicable, that the "reference spring" and "resonant frequency" methods are in good agreement.

Control of Experimental Parameters. For a given adhesion force measurement, several physical parameters may be important, including the approach/loading velocity, v_{+L}, the retraction/unloading velocity, v_{-L}, the total time in contact, t_c, the maximal load, $L_{max} = kv_{+L}t_{+L}$, and the time between the jump-out of the last adhesion experiment at the same location and the initial contact time of the current adhesion experiment, Δt. These parameters (except for t_c) are controlled using a pair of Faulhaber MCDC3006 micro motion controllers. Figure 6 shows typical hair−hair separation distance, D, and normal load, L, diagrams as functions of time, and summarizes the relevant controllable parameters and measurable variables associated with the normal motion, loading, unloading, and adhesive jumps out of the probe fiber.

Local Adhesion Force Measurements. To measure the adhesion force between two hair fibers at a given contact location, the fibers are first brought into contact at some loading velocity, v_{+L}. They are then loaded for an amount of time, t_{+L}, such that the compressive force between the surfaces reaches some maximum load, $L_{max} = kv_{+L}t_{+L}$. After

this time, the fibers are kept in contact, without loading or unloading, for an additional amount of waiting time, t_w. The hairs are then separated at some unloading velocity, v_{-L}, until they finally jump apart. The total time in contact, t_c, is calculated as the amount of time between the first contact between the fibers and the time of jump out. The fibers are separated after the jump at v_{-L} for an additional retraction time, t_r, and then held out of contact for an out-of-contact wait time, $t_{w,out}$, after which another adhesion force measurement can take place.

The values for the parameters used in the experiments presented in this work, which were kept constant for all measurements, are given in Table 2. Though not explored here, these parameters can be systematically varied to determine the dependence of the adhesion force on time and velocity, allowing us to consider relaxation processes, for example.

Spatially Resolved Adhesion Force Measurements. Due to the characteristic spatial variations in the microscopic surface structure of human hairs, caused by the semiperiodic cuticle scale geometry, there is a broad distribution in the local shape of contact points at which an adhesion measurement could take place. The adhesion between any two surfaces is also known to intimately depend on the interacting geometry and possibly the surface chemical heterogeneity. Therefore, to sufficiently sample all possible contact geometries, and therefore all possible measurable adhesion values, between a pair of hair fibers, it is important to systematically vary the relative positions of the interacting hair fibers. Given a large enough variance in the geometry, the number of measurements necessary to fully sample this distribution could be (and perhaps always is) too large to sample manually.

Therefore, for the purposes of this study, we have developed a routine to automatically perform individual adhesion experiments, according to input parameters specifying v_{+L}, v_{-L}, L_{max}, t_w, t_r, and $t_{w,out}$ while simultaneously repositioning the fibers between experiments. We define here δ_y as the overall displacement of the top (fixed) hair relative to its starting position for a series of adhesion force measurements. The algorithm for repositioning the fixed hair takes as an input half the length of the fixed hair to be sampled, $\delta_{y,max}$. Starting at the initial contact location of the first adhesion measurement in a series ($\delta_y = 0$, $D_y = D_y(t_{contact})$), the algorithm randomly chooses the direction and distance to move the fixed hair along its axis according to a random walk with a variable step size. The step distance is selected from a uniform distribution between 0 and $1/2\delta_{y,max}$. If the step would take the random walk outside of the range $\pm\delta_{y,max}$, it is reflected back into the allowed range by the remainder of the step which exceeds the maximum interval. This repositioning algorithm is repeated between each adhesion force measurement. For a given adhesive jump, the position of the probe hair along the fixed hair's axis upon separation relative to the probe hair's initial contact location on the fixed hair for the first adhesion force measurement is therefore the sum of each fibers' relative displacement, $\delta_y + \Delta D_y$, where $\Delta D_y = D_y(t_{jump}) - D_y(t_{contact})$.

This method of repositioning the hairs was chosen because as the number of experiments, N, goes to infinity, a random walk with variable step size has a uniform distribution within a given interval (as opposed
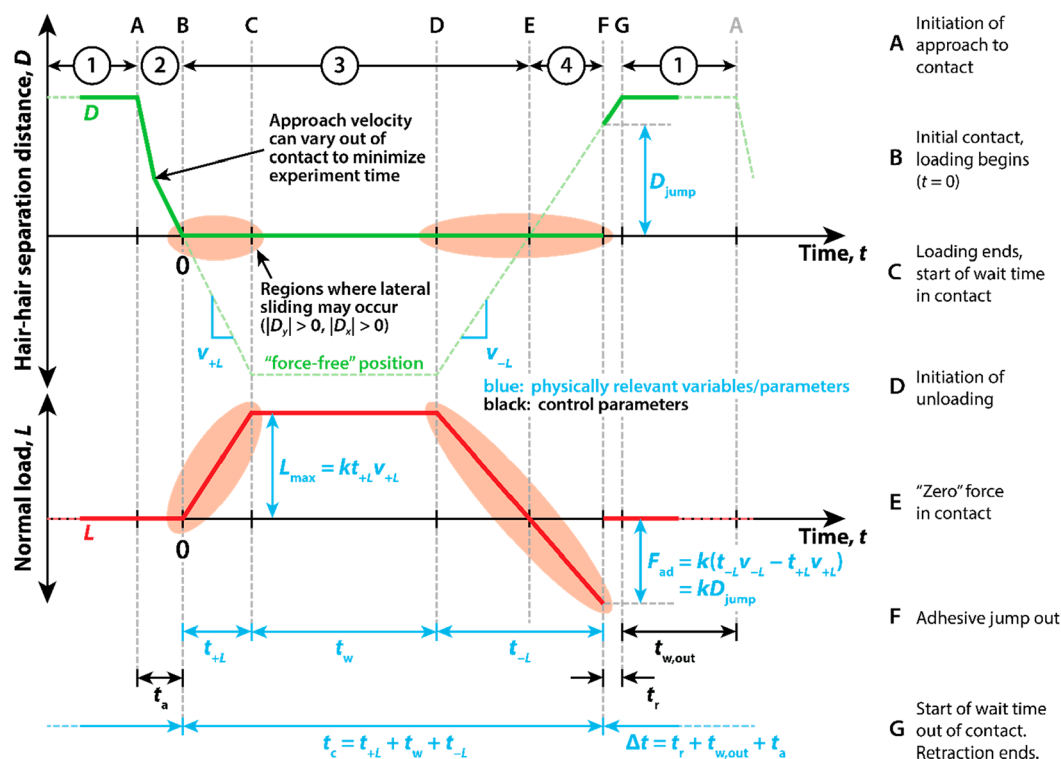
Figure 6. Schematic representation of hair–hair distance, D, and normal load, L, as a function of time, t, for a typical adhesion force measurement. The numbered time intervals correspond to the same numbered illustrations in Figure 1. The lettered time points depicted as gray dashed vertical lines correspond to the specific events indicated in the right column of labels. Parameters and variables are labeled as follows: approach/loading velocity, v_{+L}; retraction/unloading velocity, v_{-L}; approach time, t_a; loading time, t_{+L}; waiting time in contact, t_w; unloading time, t_{-L}; retraction time, t_r; waiting time out of contact, $t_{w,out}$; total time in contact, $t_c = t_{+L} + t_w + t_{-L}$; total time between experiments, $\Delta t = t_r + t_{w,out} + t_a$; maximal load, $L_{max} = kt_{+L}v_{+L}$; adhesive jump-out distance, D_{jump}; force of adhesion, $F_{ad} = k \cdot (t_{-L}v_{-L} - t_{+L}v_{+L}) = kD_{jump}$.

Table 2. Motion Parameters Used for Adhesion Force Experiments

v_{+L} (μm/s)	v_{-L} (μm/s)	L_{max} (nN)	t_w (s)	t_r (s)	$t_{w,out}$ (s)	$\delta_{y,max}$ (μm)
30 ± 2	30 ± 2	500 ± 20	3 ± 0.1	3 ± 0.1	3 ± 0.1	500

to the Gaussian or truncated-Gaussian distribution of a random walk with a uniform step size) but also maintains a small and predictable time between individual experiments when considering that repositioning the hairs is not instantaneous in practice. The random step size also ensures that there is no unintended correlation between the chosen step size and the average feature size of the hair surface. The random position selection can only automatically reposition the "fixed" hair in the presented assay, however. Repositioning both hairs is more likely to fully sample the distribution of contact geometries (discussed further in "Comparing Measured and Modeled Adhesion Force Distributions").

Measuring Surface Topography with Laser Profilometry. To estimate the effect of the hairs' surface topography on the measured adhesion force, an Olympus LEXT OLS4000 laser confocal microscope was used to obtain surface height profiles of extended regions of the hairs' surfaces containing the same regions that were contacted during the adhesion force measurements. The microscope uses laser interferometry to measure surface height with approximately 0.5 to 2 nm vertical resolution and 125 nm lateral resolution.

Each 1024 × 1024 pixel image from the microscope, at 100× magnification (0.95 NA), is a square measuring 128 μm on a side. The microscope uses an imaging wavelength of 405 nm to obtain z-stacks of interferograms, containing 300 to 700 images each, with a pitch of 60 nm. These z-stacks are used to compute a single height map at each lateral position. The microscope was programmed to acquire a series of partially overlapping height maps which, in total, cover multiple millimeters along the hairs' axes (2.6 mm for the top hairs and 0.55 mm for the bottom hairs). Using automatic feature detection, matching, and registration and affine image transformations contained in the

MATLAB Image Processing Toolbox, the acquired set of height maps were stitched together into continuous height profiles with vertical and lateral resolution equal to that of the individual images. These stitched images were further processed using an anisotropic median filter to reduce pixel spot noise and sharp features, thereby eliminating erroneously large curvatures from the topographical maps.

Simple Adhesion Force Model Based on Hair Surface Topography. Using the surface profile data acquired from laser profilometry for each pair of hairs as a function of lateral position, the local mean curvature, H, of each height map is calculated using "surfature.m", written by Daniel Claxton and available on the MathWorks MATLAB File Exchange. Figure 7 shows the surface profile of a hair segment, colored with the local mean curvature. Positive curvature (yellow) indicates convex curvature relative to the surface normal, and negative curvature (blue) indicates concave curvature relative to the surface normal. The mean curvature of the difference in height, d, between two superimposed sections of each hair is calculated in a similar fashion and is depicted in Figure 8. The curvature of this difference surface at its minimum point, d_{min}, for a given pair of superimposed sections of hair is taken as $H_{eff} = 1/R_{eff}$ for the contact between the hairs at that point. This effective radius corresponds to the radius of a "sphere-on-flat" contact which would exhibit equivalent adhesion force (given the same conditions of temperature, pressure, humidity, separation velocity, etc.). To a first approximation, the adhesion force is therefore given by
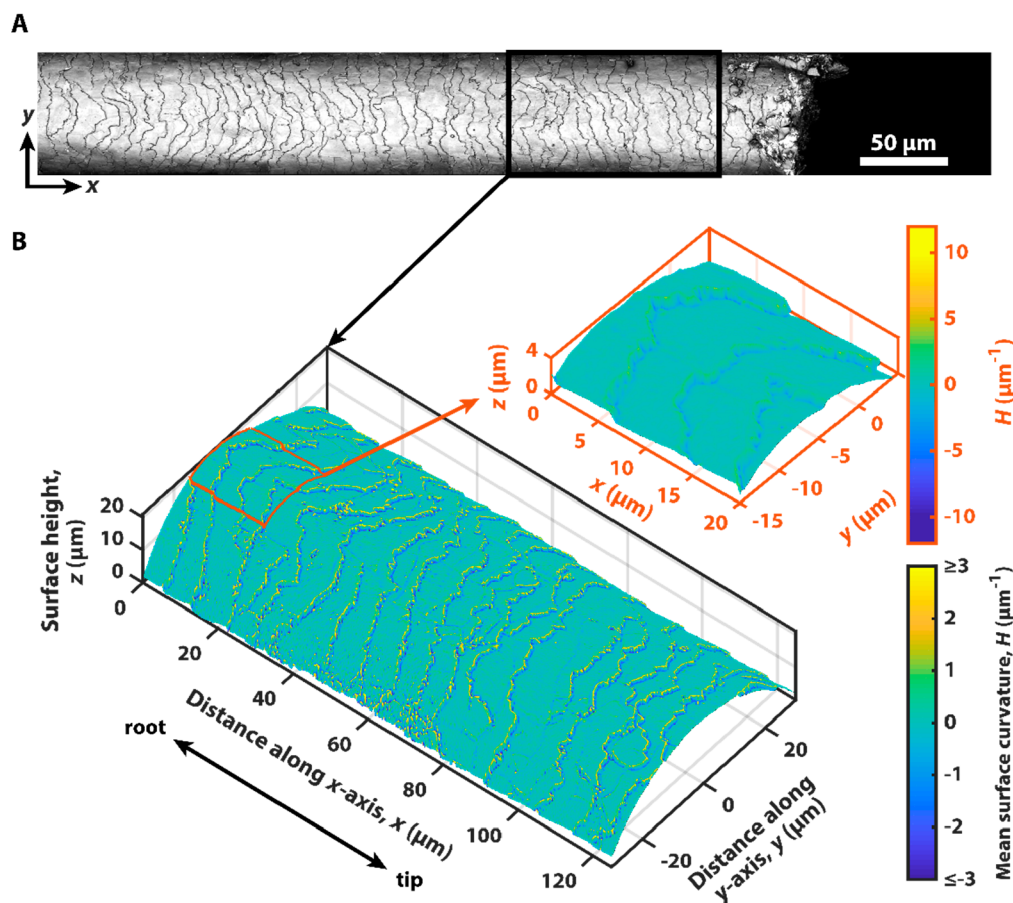
$$F_{ad} = -4\pi R_{eff}\gamma$$

Figure 7. Hair surface topography from laser confocal microscopy. (A) Optical micrograph from laser confocal microscope depicting ∼400 μm near the tip of the probe hair segment of Clean Hair 8. (B) The larger plot shows the ∼125 μm long surface height map from the boxed region of the image in panel (A) with the coloration corresponding to the local mean curvature at each point. The color scale in the larger image is saturated at both positive and negative curvature to give higher contrast to the surface features. The zoomed orange inset corresponds to the outlined region on the larger plot and has a full color scale with no saturation.

where F_{ad} is the force of adhesion between the two surfaces at a given contact point (negative forces are adhesive, positive forces are repulsive) and γ is the average surface energy of the hair, which has been measured previously using a fiber tensiometer.[8,27] For the purposes of this model, we will assume $\gamma = 26$ mJ/m², as measured for clean hair.[8,27] The treatment used for the treated hairs in this study is not known to dramatically change the overall surface energy, and therefore, $\gamma = 26$ mJ/m² is used for these experiments as well. Models of other treatments may require a different surface energy to best fit the measured adhesion force data.

Using this simplified model, the spatial and overall distribution of randomly sampled adhesion forces has been calculated for selected subregions of the imaged hair surfaces by calculating F_{ad} for each possible relative lateral position. The dimensions of the sub sections used to calculate each modeled adhesion force distribution correspond to the real physical dimensions of the adhesion force measurements. For example, if the fixed hair was automatically translated within a 1 mm sampling range during the adhesion force measurements, and the probe hair was observed to translate 15 μm along its axis due to its own natural bending, then the simulated adhesion distributions would be calculated by comparing each permutation of the two hair images within 1 mm on the top hair and 15 μm on the bottom hair.

RESULTS AND DISCUSSION

Reproducibility of Local Adhesion Force Measurements. By following the protocol detailed in "Local Adhesion Force Measurements", the adhesion force between two hair

fibers has been repeatedly measured within the same approximate contact region (± 2 to 5 μm) along each fiber's axis. From these localized experiments, the measured adhesion force may either be highly reproducible and approximately single-valued, or exhibit several distinct, reproducible modes. This is best demonstrated in Figure 9, which shows six replicate adhesion force measurements, acquired during HAFA development and testing, whose jump distances (and therefore adhesion forces) modulate between two distinct values. Each of the two jump distances is highly reproducible, shown in Figure 9A, and correspond to specific lateral positions, D_y, along the fixed hair (Figure 9B).

To explain the observed multimodal behavior in adhesion force, we note that, due to nonidealities in the probe hair's shape, including variations in diameter, ellipticity, twist angle, internal composition, cuticle thickness, and spatial cuticle density, it is challenging, if not impossible, to determine a single major bending mode for a given fiber. Therefore, upon application of increased compressive force (L) between the hair fibers after contact, the position of the probe hair along the axis of the fixed hair (D_y) relative to its initial contact position may translate slightly ($<20 \mu$m). This allows the probe hair to sample different areas of the fixed hair during loading and unloading. We believe, therefore, that the differences in the modes of adhesion force correspond to the different geometries of different local minima
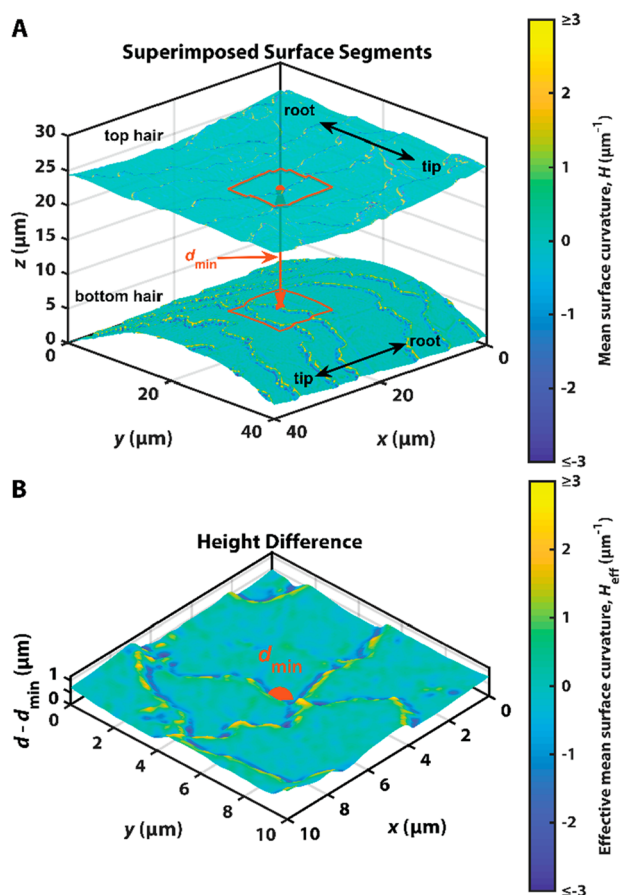
Figure 8. Schematic demonstration of calculating R_{eff} using differential geometry. (A) Two surface height maps, colored by their local mean curvature, H, from sections of two separate hairs superimposed with their root-to-tip axes oriented at 90°. The external surfaces of the hairs are facing each other; therefore, the "top hair" height data has been rotated 180° about the y-axis after acquisition. The point of closest approach, d_{min}, is indicated with an orange circle on each hair and an orange double arrow. The difference in height, d, within the orange, outlined regions on each surface is shown in (B). (B) Surface plot of the difference in height between the top and bottom hairs, colored by local mean curvature of this difference surface, H_{eff}, within a region near the point of closest approach, d_{min}. $H_{eff}(d_{min})$ is assumed to be the effective "sphere-on-flat" curvature at the point of closest approach, used to model the force of adhesion between the hairs at that point. The model computes this curvature for thousands of different relative positions of the top and bottom hairs.

in the overlapping hairs' surface structures in which the probe hair may get trapped within its sliding path during unloading. These different local geometries have different effective radii of contact, R_{eff}, assuming a single-asperity model, and, given the cuticle structure of hair fibers, can result in orders of magnitude variations in adhesion force, F_{ad}, for a single pair of fibers (even if the surface energy of the hair, γ, is assumed to be spatially invariant).

When sampling small enough areas, like in the case where the relative hair positions are not intentionally varied between measurements, the effect of surface topography will result in only a few distinct modes in the adhesion force histogram associated with the small set of local adhesive minima available to the probe hair in that area.

Effect of Contact Location on Adhesion Force. Given the multimodal nature of the adhesion force between the hair fibers and the assumption that these modes arise from heterogeneities in the surface structure (and chemistry) of both the probe and fixed hairs, it is necessary to randomly sample the local adhesion force over large sections of hair (>500 μm) using thousands of individual measurements in order to fully characterize the adhesion force between two fibers. This is accomplished by repositioning the top fiber along its cylindrical axis between individual measurements (discussed further in "Spatially Resolved Adhesion Force Measurements"). Because of the loosely correlated nature of the cuticle edge separation distance along the axes of hair fibers, the new position of the fiber after a given adhesion force measurement is chosen using a random walk with variable step size. This choice limits the potential for oversampling the same type of location, be it cuticle edge or cuticle flat, along the hair fiber, which could be common if a uniform step size was chosen which correlates well with the average intercuticle distance.

This series of adhesion measurements for a given pair of hairs, in combination with simultaneous tracking of the relative positions of the probe and fixed fibers, allows us to develop overall (Figure 10) and spatially resolved (Figure 11) adhesion force histograms which fully characterize the expected probability distribution of adhesion forces within the length of hair measured. The overall distributions in Figure 10, though somewhat varied in their shape, are all within the same range of forces (0 to ~1500 nN) and have similar breadths. It is also universal, regardless of the overall shape, for each distribution to have at least one mode in the 100 to 200 nN range, with additional modes, like those seen in Clean Hairs 6 and 7, potentially extending above 500 nN.

We observe a mostly uniform spatial adhesion force distribution, however, there are regions in which a particular mode of adhesion force may dominate. This spatial modality is most easily observed for Clean Hair 7 (Figure 11A). The lower and higher modes in the overall adhesion distribution are localized in space between −400 and −200 μm and between 100 and 400 μm, respectively. Other more subtle spatial variations are observed in the distributions in Figure 11B,C. Though not depicted here, changing the contact region on the probe hair by manually translating it along its axis between a series of experiments causes subtle changes in the overall adhesion distribution. Because of this effect, we believe that future implementations of the HAFA should include the ability to automatically translate the probe hair as well. The adhesion force model presented in "Simple Adhesion Force Model Based on Hair Surface Topography" and "Comparing Measured and Modeled Adhesion Force Distributions" further corroborates this conclusion. Due to the density of the data, the bin size chosen to generate the histograms also has minimal effect.

This rich information allows for confident coarse-graining of the adhesion distribution and can be applied in models of full heads of hair[15] by selecting a random sample of adhesion forces from the measured distribution for each simulated hair–hair contact.

Comparing Measured and Modeled Adhesion Force Distributions. The surface topography of the HAFA contact regions of each of the four pairs of hair segments presented in Figure 11 has been measured ex situ according to the procedure detailed in "Measuring Surface Topography with Laser Profilometry". With this topographical information, the adhesion force between the probe and fixed fiber segments has
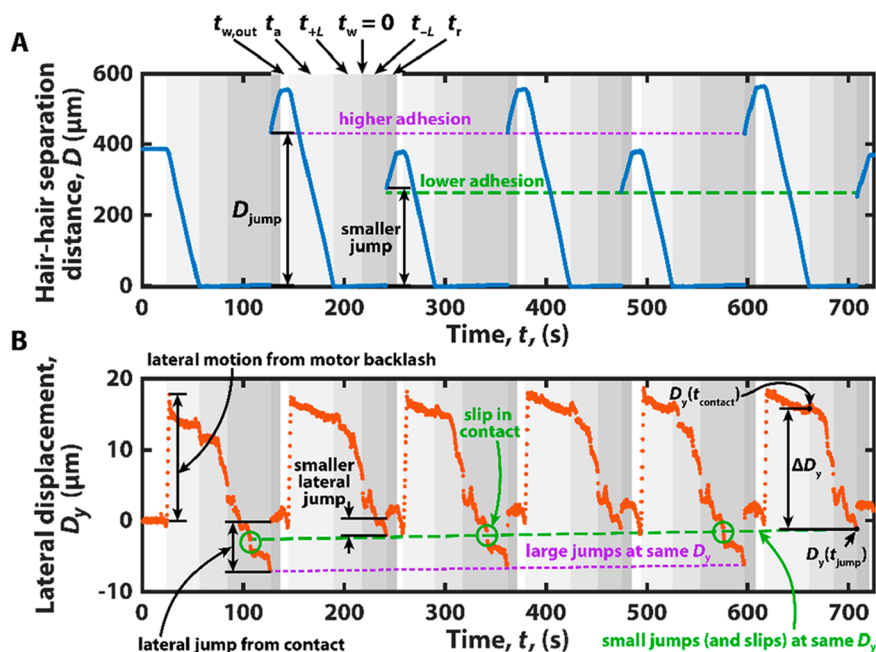
Figure 9. Characteristic D and D_y traces during a series of adhesion force measurements. (A) Hair separation distance, D, plotted as a function of time, t. The automation segments, labeled with their respective time intervals, are indicated in various shades of gray. There are two distinct modes of D_{jump} (and therefore adhesion force) present during this experiment, labeled with black double arrows and classified by the purple and green (short and long) dashed lines. (B) The lateral displacement of the probe hair segment, D_y, plotted as a function of time, t, for the same trace in (A). Lateral jumps of the probe hair upon jump out are labeled with black arrows. The lateral location corresponding to the two different modes in D_{jump} are reproducible and indicated with purple and green (short and long) dashed lines. Lateral slips in the D_y traces during the higher-adhesion cycles are circled in green and align with the lateral jumps of the lower-adhesion cycles.
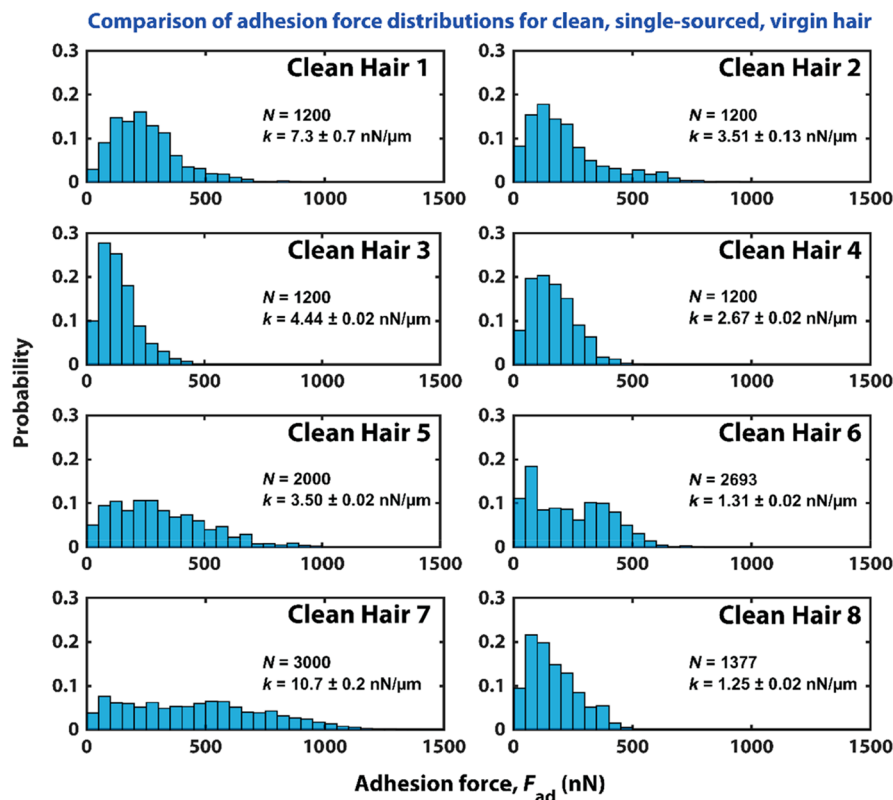

Figure 10. Overall adhesion force histograms for eight pairs of clean, virgin hairs sourced from the same individual. All experiments were conducted at ~62 ± 1% relative humidity and ~24 ± 0.5 °C with motion parameters given in Table 2.
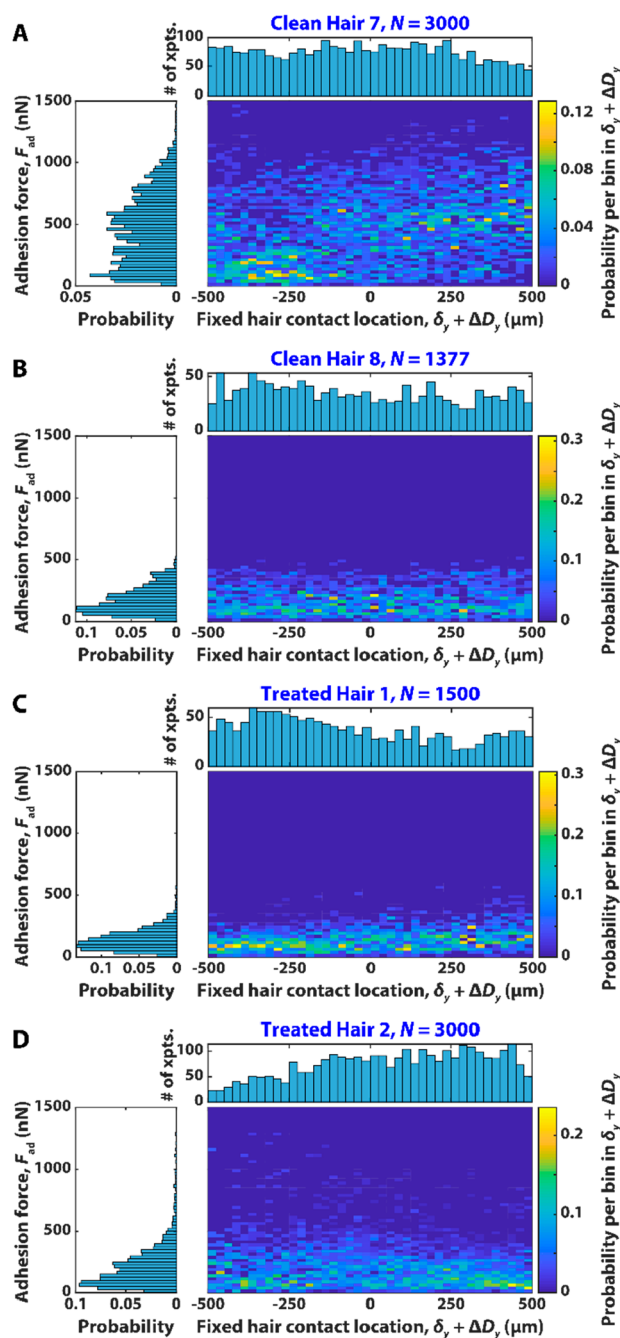
Figure 11. Spatially resolved adhesion force distributions for (A, B) clean and (C, D) treated hair specimens. The 2D histogram plots the probability of measuring a particular adhesion force (vertical bins) within a range of locations along the fixed hairs length (horizontal bins). The top bar chart of each panel shows how many individual ahdesion measurements were conducted within a particular horizontal bin. The left, rotated, 1D histogram in each panel shows the overall probability, averaged along the fixed hairs length, of measuring a particular adhesion force for the given pair of hairs.

also been modeled according to the procedure in "Simple Adhesion Force Model Based on Hair Surface Topography". The resulting overall adhesion force histograms calculated by superimposing the full image range of the model are presented in orange in the top plots panels A−D in Figure 12. The full image range from the topographical data over-represents the length-scales measured in the HAFA, but already begins to reproduce

the main features of the empirical adhesion force distributions. For example, the overall range in forces, from approximately 1 to 1000 nN is well represented in the model. The right tails of the "full-image" model distributions extend to very high forces and slowly decay to zero probability. This asymptotic behavior is impossible to fully reproduce in the physical experiments with such small N, but the measurements do suggest an extended, high-adhesion force tail would be observed. The model histograms also have major peaks around 100 to 200 nN in all cases, which is in good agreement with the measured distributions and have similar spatial variations in adhesion force, as demonstrated in the right-hand panels of Figures S9− S12 in the SI.

Finally, the model distribution for "Clean Hair 7" in Figure 12A reproduces a large shoulder, extending to >350 nN. We believe this shoulder, observed in both the measured adhesion force distribution and the model distribution, exists because the cross section of "Clean Hair 7" was more "bean-shaped" than elliptical. This is most readily noticeable from the horizontal hair image in Figure S1 in the SI. Along the entire length of the top hair, there is a macroscopically concave feature, not only giving the hair low curvature within that feature, but also causing there to be two separate convex curvature regions for any given position along the hair's axis. This complex morphology might be characteristic in a given individual's head of hair, and we believe that instead of avoiding nonideal geometries due to their difficulty to measure, it is best to characterize all possible manifestations of the hair system. Both the HAFA technique and the adhesion model can capture these complexities equally well.

To even better represent the measured histograms using the surface topography model, the model distributions have been subsectioned into relevant length scales of each hair fiber (1000 μm along the top hair and 10−35 μm on the bottom hair). When subdividing the "full image range" distributions into smaller sections, we can compute for each subsection's overall histogram a statistical parameter, "Y^2",[29] which captures the goodness of fit between two randomly sampled, binned distributions (the model and HAFA adhesion force distributions in this case). The statistical parameter is a modified version of Karl Pearson's χ^2 parameter for determining goodness of fit between categorical distributions, which has been adapted to better represent comparisons between histograms which have some bins with counts ≤10. For a two-sample test[30] of multinomial distributions (like the data we have generated with the HAFA and the model), the parameter takes the following form:

$$Y^2 = \nu + \sqrt{\frac{2\nu}{2\nu + \left[\frac{(R+S)^2}{RS} - 6\right]\sum_{i=1}^{N_B}\frac{1}{R_i + S_i}}}\left(\sum_{i=1}^{N_B}\frac{\left(\sqrt{\frac{S}{R}}R_i - \sqrt{\frac{R}{S}}S_i\right)^2}{R_i + S_i} - \nu\right)$$

where N_B is the total number of bins containing >0 counts for both distributions, R_i and S_i are the histogram counts in the ith bin for each distribution, and ν is the number of degrees of freedom, which is equal to $N_B - 1$ for this system having no fitting parameters. Finally, R and S are the total number of counts in each distribution:

$$R = \sum_{i=1}^{N_B} R_i \quad S = \sum_{i=1}^{N_B} S_i$$

Computing the Y^2 parameter also allows for the calculation of a p-value between the two distributions to determine whether they are significantly different. However, given the size of the distributions ($R > 1000$ for the measured distributions and $S >$
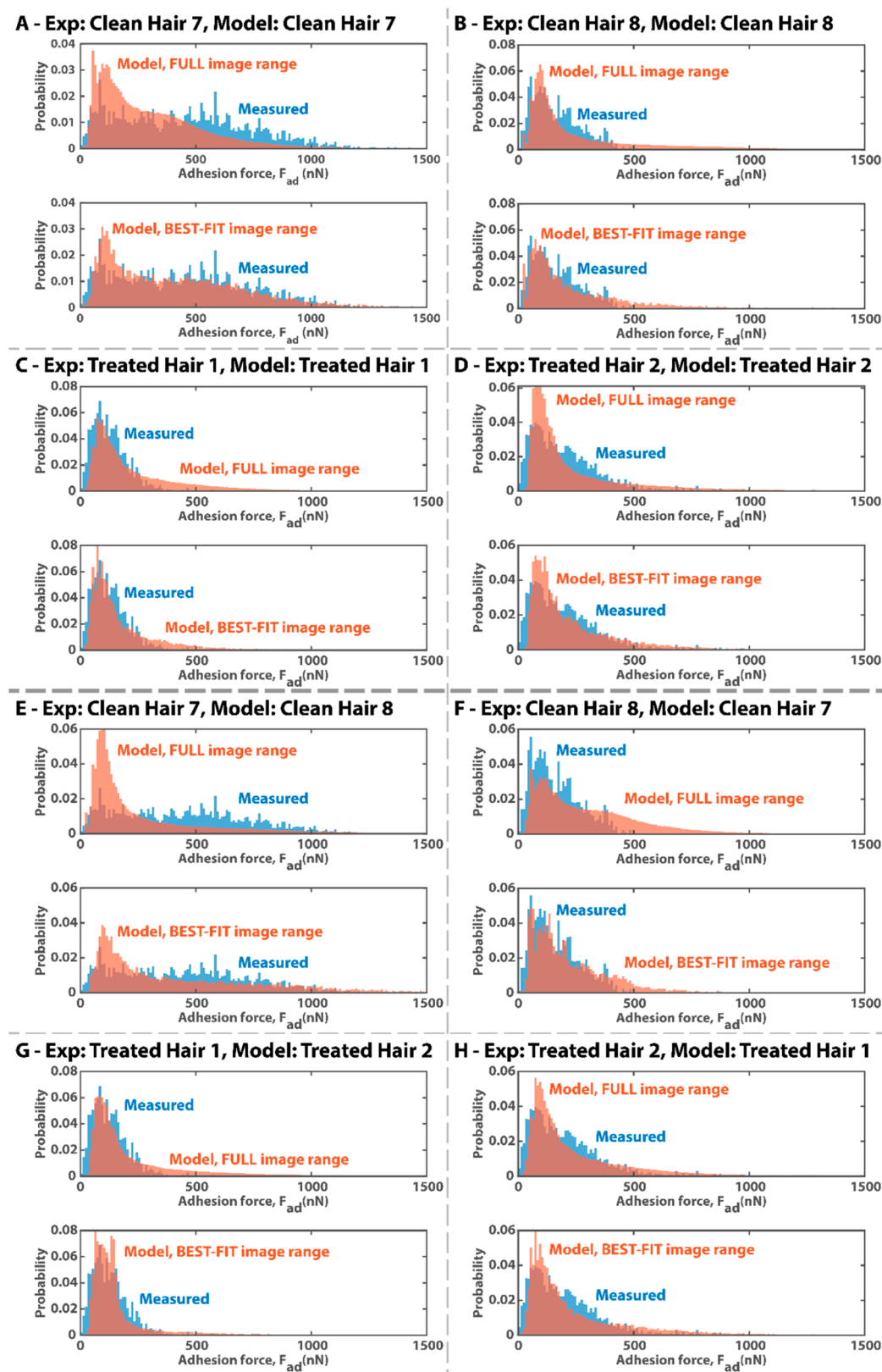
Figure 12. Comparison of experimentally measured adhesion forces using HAFA (Exp) and modeled adhesion forces using surface topography (Model) for the four hair samples studied in this work (clean, A, B, E, and F; treated C, D, G, and H). For each main panel A—H, the top subpanel shows the model histogram calculated using the full range of acquired profilometry data, while the bottom subpanel shows the model histogram calculated using the best-fit sub sections of each fixed/probe hair which correspond to the physically relevant lengths of hair measured during the HAFA experiments. Panels A—D show comparisons where the HAFA and profilometry data come from the same hairs while panels E—F compare experiment/model data from dissimilar hairs to demonstrate the robustness of the model.

400000 for the model distributions), the *p*-value always reports that the distributions are different. Nevertheless, we can still use the calculated Y^2 for each physically relevant spatial subsection of the model distribution to find the "best-fit" subsection where the model and measured data agree most strongly. This "best-fit" subsection will reside where Y^2 is at its minimum. Figures S1−S4 in the SI plot the Y^2 parameter as a function of location along the hair images for each of the four hairs studied in this work. The minimum Y^2 parameter is indicated and the overall adhesion force distribution associated with this minimum Y^2 parameter is plotted in the bottom panels of Figure 12A−D.

The "best-fit" distributions better represent the shapes of the measured distributions. We believe this is because they are sampled from physically relevant lengths of hair. The most striking resemblance is found again for Clean Hair 7 in the bottom panel of Figure 12A. The shoulder from the model distribution almost perfectly matches the second mode in the measured distribution, though the lower forces are still over-represented in the model. The agreement between the "best-fit" modeled and measured distributions, though encouraging, does not imply that we have found, using this model, the true location along the probe and fixed hairs from which the measured distributions have been sampled. We can conclude, however, that the model verifies the notion that there exists a combination of surface topographies for a given pair of hair segments which can, using no free fitting parameters (the surface energy, γ, of 26 mJ/m^2 is fixed), predict the general shape and magnitude of the measured distributions.

We have also compared the measured adhesion force distributions to the modeled distributions from different hair surfaces to study if similar results can be obtained for models which could not have contained the same surface topographies as the lengths of hair studied in the HAFA. The results from these "cross-comparisons" are shown in Figure 12E−H and Figures S5−S8 and S14−S16 in the SI. These plots are all identical to the direct comparisons described above; however, the pairing of modeled to measured distributions has been switched (comparing HAFA data from Clean Hair 7 to the surface topography model from Clean Hair 8, for example). The major conclusion from this "cross-comparison" study is that "best-fit" model distributions tend to sacrifice overall shape for better agreement with the mean of the distribution. After obtaining these cross-comparisons, it is most useful to compare the bottom "best-fit" panels to their direct-comparison counterparts (comparing Figure 12A to E, B to F, C to G, and D to H). For all cross-comparisons but the one between measured Clean Hair 7 and modeled Clean Hair 8, it is difficult from inspection to determine whether the direct- or cross-comparison is a better fit for the HAFA data. However, again, the complicated shape of the Clean Hair 7 morphology caused the HAFA adhesion for distribution to only be best represented by the model distribution obtained from the same hairs. Though the "best-fit" model distribution from Clean Hair 8 for the measured distribution from Clean Hair 7 (Figure 12E, bottom panel) has an extended tail, it cannot capture the shape of the higher mode of adhesion from the HAFA measurements.

Because the model and measurements agree well when applied over the same length scales of hair, it is satisfying to assume that if the probe hair, in addition to the fixed hair, were randomly and automatically translated along its axis between individual adhesion force measurements, the measured adhesion force distributions would converge to the "full-image range" model distributions, given enough replicate measurements.

However, a few caveats remain in this assumption: (i) the surface topography model treats all surface features as infinitely rigid asperities, (ii) if the surfaces contact at a very high curvature, localized asperity (like that associated with a contaminant or a highly raised cuticle edge), the model does not allow for the surfaces to readjust their positions to slide past the asperity, (iii) similarly, though each surface is locally planarized with respect to the $x-y$ plane preceding each R_{eff} calculation, the height maps are not planarized with respect to one another, (iv) the surfaces are not allow to translate laterally until they find the closest local minimum in surface curvature for a given R_{eff} calculation. These caveats preclude the model from perfectly representing the measured distributions, and in effect cause the model to over-represent lower radius (lower adhesion force, higher energy) contacts. Future work to account for these limitations would prove useful.

■ SUMMARY AND CONCLUSIONS

Using a specially designed modification to an SFA Mark II, dubbed the "hair adhesion force apparatus" (HAFA), we can measure the overall and spatial distributions in adhesion force between individual human hair fibers with ∼1 nN force resolution and ∼1 μm spatial resolution (in one dimension). The technique is the first example of using the hair fibers themselves to determine the surface forces. This approach is easier to implement than similar AFM-based adhesion force measurements and allows the hairs to bend naturally with the forces that would be present in the native environment within a head of hair. We find that, universally, for the clean and treated samples measured in this study, which do not have significant surface modifications compared to a natural hair surface, there exists at least one mode of adhesion force within 100−300 nN (or corresponding to local curvatures of ∼1−2 μm). Additional modes may also be present, depending on the surface geometry of the hair.

Making only a single assumption about the surface energy of the hair fibers, an adhesion force model, which considers the ex situ-determined surface topography of the hairs measured in the HAFA, can predict the magnitude, range, and shape of the measured adhesion force distributions. More careful statistical considerations allow for the model to capture subtleties in the distributions with adequate fidelity. The combination of these two techniques gives further insight into just how important the surface features of hair fibers can be in modulating the adhesion within a full head of hair. Perhaps from these experiments, novel hair care products that attempt to directly control surface morphology can be developed. Finally, the distributions obtained in this work may provide a foundation for more complex models of full heads of hair, which can coarse-grain these phenomena by sampling from distributions with similar shapes.

■ ASSOCIATED CONTENT

ⓢ Supporting Information

The Supporting Information is available free of charge on the ACS Publications website at DOI: 10.1021/acs.langmuir.9b02033.

Figures S1−S16 (PDF)

■ AUTHOR INFORMATION

Corresponding Author

*E-mail: trcristiani@gmail.com. Tel.: +1 (908) 418-8665.

ORCID ⬤

Thomas R. Cristiani: 0000-0003-3303-7865
Kai Kristiansen: 0000-0002-7555-9437
Peter H. Koenig: 0000-0002-6512-5686
Jacob N. Israelachvili: 0000-0001-8915-8741

Present Addresses

‖Author's current address is different than affiliation.
#Department of Materials Science and Engineering, University of California, Merced, CA 95344, U.S.A.

Author Contributions

The manuscript was written through contributions of all authors. All authors have given approval to the final version of the manuscript.

Notes

The authors declare no competing financial interest.
△This author is deceased.

■ REFERENCES

(1) Chen, N.; Bhushan, B. Morphological, nanomechanical and cellular structural characterization of human hair and conditioner distribution using torsional resonance mode with an atomic force microscope. *J. Microsc.* **2005**, *220*, 96−112.

(2) Latorre, C.; Bhushan, B. Nanotribological effects of hair care products and environment on human hair using atomic force microscopy. *J. Vac. Sci. Technol., A* **2005**, *23*, 1034.

(3) Gray, J. Hair care and hair care products. *Clin. Dermatol.* **2001**, *19*, 227−236.

(4) Bhushan, B. *Biophysics of Human Hair*; Springer Berlin Heidelberg: Berlin, Heidelberg, 2010.

(5) Bhushan, B. Nanoscale characterization of human hair and hair conditioners. *Prog. Mater. Sci.* **2008**, *53*, 585−710.

(6) LaTorre, C.; Bhushan, B. Nanotribological characterization of human hair and skin using atomic force microscopy. *Ultramicroscopy* **2005**, *105*, 155−175.

(7) Wei, G.; Bhushan, B.; Torgerson, P. M. Nanomechanical characterization of human hair using nanoindentation and SEM. *Ultramicroscopy* **2005**, *105*, 248−266.

(8) Lodge, R. A.; Bhushan, B. Wetting properties of human hair by means of dynamic contact angle measurement. *J. Appl. Polym. Sci.* **2006**, *102*, 5255−5265.

(9) Seshadri, I. P.; Bhushan, B. Effect of ethnicity and treatments on in situ tensile response and morphological changes of human hair characterized by atomic force microscopy. *Acta Mater.* **2008**, *56*, 3585−3597.

(10) Bhushan, B.; Chen, N. AFM studies of environmental effects on nanomechanical properties and cellular structure of human hair. *Ultramicroscopy* **2006**, *106*, 755−764.

(11) Seshadri, I. P.; Bhushan, B. In situ tensile deformation characterization of human hair with atomic force microscopy. *Acta Mater.* **2008**, *56*, 774−781.

(12) Wei, G.; Bhushan, B. Nanotribological and nanomechanical characterization of human hair using a nanoscratch technique. *Ultramicroscopy* **2006**, *106*, 742−754.

(13) LaTorre, C.; Bhushan, B. Investigation of scale effects and directionality dependence on friction and adhesion of human hair using AFM and macroscale friction test apparatus. *Ultramicroscopy* **2006**, *106*, 720−734.

(14) Bhushan, B.; Wei, G.; Haddad, P. Friction and wear studies of human hair and skin. *Wear* **2005**, *259*, 1012−1021.

(15) Michels, D. L.; Mueller, J. P. T.; Sobottka, G. A. A physically based approach to the accurate simulation of stiff fibers and stiff fiber meshes. *Comput. Graph.* **2015**, *53*, 136−146.

(16) Max, E.; Häfner, W.; Wilco Bartels, F.; Sugiharto, A.; Wood, C.; Fery, A. A novel AFM based method for force measurements between individual hair strands. *Ultramicroscopy* **2010**, *110*, 320−324.

(17) Luengo, G. S.; Mizuno, H.; Rutland, M. W. *Hair−Hair Contact Dynamics and Interactions Studied with Atomic Force Microscopy*; Springer International Publishing: Cham, 2017.

(18) Mizuno, H.; Luengo, G. S.; Rutland, M. W. Interactions between crossed hair fibers at the nanoscale. *Langmuir* **2010**, *26*, 18909−18915.

(19) Mizuno, H.; Luengo, G. S.; Rutland, M. W. New Insight on the Friction of Natural Fibers. Effect of Sliding Angle and Anisotropic Surface Topography. *Langmuir* **2013**, *29*, 5857−5862.

(20) Adams, M. J.; Briscoe, B. J.; Wee, T. K. The differential friction effect of keratin fibres. *J. Phys. D: Appl. Phys.* **1990**, *23*, 406−414.

(21) Adams, M. J.; O'Keefe, E.; Briscoe, B. J.; Kremnitzer, S. L. A study of the friction and adhesion of polyethylene-terephthalate monofilaments in liquid media. *J. Phys. D: Appl. Phys.* **1983**, *16*, L9−L15.

(22) Briscoe, B. J.; Kremnitzer, S. L. A study of the friction and adhesion of polyethylene-terephthalate monofilaments. *J. Phys. D: Appl. Phys.* **1979**, *12*, 505−516.

(23) Pascoe, M. W.; Tabor, D. The Friction and Deformation of Polymers. *Proc. R. Soc. A Math. Phys. Eng. Sci.* **1956**, *235*, 210−224.

(24) Israelachvili, J.; Min, Y.; Akbulut, M.; Alig, A.; Carver, G.; Greene, W.; Kristiansen, K.; Meyer, E.; Pesika, N.; Rosenberg, K.; Zeng, H. Recent advances in the surface forces apparatus (SFA) technique. *Rep. Prog. Phys.* **2010**, *73*, 036601.

(25) Torii, A.; Sasaki, M.; Hane, K.; Okuma, S. A method for determining the spring constant of cantilevers for atomic force microscopy. *Meas. Sci. Technol.* **1996**, *7*, 179−184.

(26) Cumpson, P. J.; Hedley, J.; Zhdan, P. Accurate force measurement in the atomic force microscope: a microfabricated array of reference springs for easy cantilever calibration. *Nanotechnology* **2003**, *14*, 918−924.

(27) Wortmann, F. J.; Wortmann, G.; Schulze zur Wiesche, E. Spatial Probing of the Properties of the Human Hair Surface Using Wilhelmy Force Profiles. *Langmuir* **2010**, *26*, 7365−7369.

(28) Irvine, T. Application of the Newton-Raphson Method to Vibration Problems, Revision E; Vibrationdata.com.

(29) Lucy, L. B. Hypothesis testing for meagre data sets. *Mon. Not. R. Astron. Soc.* **2000**, *318*, 92−100.

(30) Press, W. H.; Teukolsky, S. A.; Vetterling, W. T.; Flannery, B. P. *Numerical Recipes in C*; Cambridge University Press: Cambridge, 1982.